Journal Pre-proof

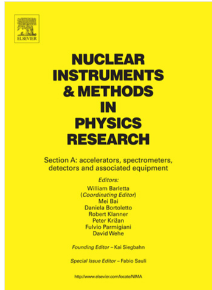

Image quality determination of a novel digital detector for X-ray imaging and cone-beam computed tomography applications

Hanan Alzahrani, Sion Richards, Iain Sedgwick, Paul Seller,
Anastasios Konstantinidis, Gary Royle, Kate Ricketts

PII: S0168-9002(20)30402-2
DOI: https://doi.org/10.1016/j.nima.2020.163914
Reference: NIMA 163914

To appear in: *Nuclear Inst. and Methods in Physics Research, A*

Received date : 13 November 2019
Revised date : 11 February 2020
Accepted date : 7 April 2020

Please cite this article as: H. Alzahrani, S. Richards, I. Sedgwick et al., Image quality determination of a novel digital detector for X-ray imaging and cone-beam computed tomography applications, *Nuclear Inst. and Methods in Physics Research, A* (2020), doi: https://doi.org/10.1016/j.nima.2020.163914.

This is a PDF file of an article that has undergone enhancements after acceptance, such as the addition of a cover page and metadata, and formatting for readability, but it is not yet the definitive version of record. This version will undergo additional copyediting, typesetting and review before it is published in its final form, but we are providing this version to give early visibility of the article. Please note that, during the production process, errors may be discovered which could affect the content, and all legal disclaimers that apply to the journal pertain.

© 2020 Published by Elsevier B.V.

the revised manuscript

Journal Pre-proof

Image Quality Determination of a Novel Digital Detector for X-ray Imaging and Cone-Beam Computed Tomography Applications

Hanan Alzahrani[1, 2*], Sion Richards[3] Iain Sedgwick[3], Paul Seller[3], Anastasios Konstantinidis[4], Gary Royle[5], Kate Ricketts[1]

Journal Pre-proof

[*] Corresponding author. e-mail: hanan.alzahrani.13@ucl.ac.uk.

Journal Pre-proof

[1]Research Department of Tissue and Energy, Division of Surgery and Interventional Science, University College London, London, W1W 7TS, U.K.

[2]Applied Medical Science Faculty, Taibah University, Medina, 42353, Saudi Arabia.

[3]Science and Technology Facilities Council, Rutherford Appleton Laboratory, Harwell Campus, Didcot, OX11 0QX, U.K.

[4]Diagnostic Radiology and Radiation Protection, Christie Medical Physics and Engineering, The Christie NHS Foundation Trust, Manchester, M20 4BX, U.K.

[5]Department of Medical Physics and Biomedical Engineering, University College London, London, WC1E 6BT, U.K.

Abstract

The demand for adequate image quality with low radiation doses for patients has greatly increased. This is especially true in the case of position verification in radiotherapy which requires a high number of images per patient. This study presents a physical characterisation of a new clinical detector named “Lassena (CsI)” based on a thick layer of structured thallium activated caesium iodide and complementary metal-oxide semiconductor technology with active pixel sensor architecture for general X-ray imaging and cone-beam computed tomography (CBCT) applications. We made a critical appraisal of its performance for the first time and determined its signal transfer property (STP) and its detective quantum efficiency (DQE) by acquiring the pre-sampling modulation transfer function (pMTF) and normalised noise power spectrum (NNPS) in addition to the dark current calculation. The investigation was conducted with the application of three X-ray beam qualities: (50 kV (RQA3), 70 kV (RQA5) and 90 kV (RQA7)) in compliance with the International Electrotechnical Commission (IEC 62220-1(2003)) standard. The STP was found to be linear with the coefficient of determination (R^2) more than 0.9995 in all cases. The spatial resolution and NNPS results led to acceptable DQE values at all energies; in particular the DQE values at 0.5 line pairs per mm (DQE(0.5)) which were 0.46 for RQA3, 0.52-0.56 for RQA5 and 0.55-0.59 for RQA7. Lastly, the dark current was 2.51 pA/cm^2 for a 50 μm pixel pitch. For CBCT applications, Lassena (CsI) showed very promising results.

Keywords: signal-to-noise ratio, image quality, DQE, detector characterisation.

1. Introduction

Digital X-ray detectors have gained widespread use in clinical applications. This is due to their high degree of performance and accuracy which can be quantified using the detective quantum efficiency (DQE) parameter to indicate the image system performance as it varies from one system to another [1-5]. In general, the DQE describes the transmission of the signal to noise ratio (SNR) in X-ray imaging detectors taking into account the spatial resolution and noise [5,6]. An ideal imaging system would have a DQE value of one at all spatial frequencies. In all practical cases, however, the DQE decreases as a function of spatial frequency due to the increased effect of the noise as a function of spatial frequency [6,7]. The other two criteria of the image quality assessment are pre-modulation transfer function (pMTF) and normalised noise power spectrum (NNPS). The pMTF indicates the image resolution and the spatial frequency corresponding to 10% of pMTF is frequently used to

Journal Pre-proof

express the limiting resolution of the system [7]. In general radiography, the adequate limiting resolution for a radiation detector ranges between 3 and 5 line pairs per millimetre (lp/mm) [8]. The NNPS is one of the popular metrics providing a quantitative description for the noise variance in an imaging system as a function of spatial frequency [9].

Digital radiation detectors based on complementary metal-oxide semiconductor (CMOS) technology are becoming prevalent since they offer low voltage operation, low power consumption and low cost while maintaining acceptable image quality [10,11]. In particular, CMOS sensors based on the active pixel sensor (APS) structure as they allow in-pixel buffering of the signal and therefore they have better image quality [11].

The properties of the scintillator and its thickness have an impact on the image quality as well. X-ray imaging detectors commonly use a powdered scintillator also known as a phosphor such as gadolinium oxysulfide doped with terbium also known as Gadox or P43 in a polymer matrix or caesium iodide doped with thallium (CsI(Tl)). Both scintillators have large conversion gains and their peak emission wavelength is in the green portion of the visible spectrum at 550 nm for CsI(Tl) and 545 nm for Gadox which matches the peak quantum efficiency of silicon based sensor resulting in a high signal collection. CsI(Tl) can be grown to have a micro-columnar structure which reduces the laterally spread of the scintillation light resulting in greater spatial resolution than phosphor screens. Increasing the thickness of the scintillator leads to higher X-ray absorption but any scintillation light generated at the top of the scintillator will spread more resulting in lower spatial resolution and higher noise [11-14].

The purpose of this work is a characterisation of a new radiation detector through physical figures of merit (pMTF, NNPS, and DQE) and proposing it as a radiation detector for general radiographic imaging and cone-beam computed tomography (CBCT) applications which play an essential role in image-guided radiation therapy (IGRT) and adaptive radiotherapy (ART) aspects.

2. Materials and Methods

The detector under investigation which is referred to as “Lassena (CsI)” is a three transistor (3T) wafer-scale CMOS APS designed by The Science and Technology Facilities Council’s Rutherford Appleton Laboratory (RAL, Oxford, UK). It is coupled to a 1000 µm CsI(Tl) scintillator to convert incident X-ray photons into optical light. CsI (TI) is used in medical imaging due to its high resolution and low noise [6, 7]. A thicker layer of CsI (Tl) was used with this Lassena sensor to improve its efficiency at low doses. However, this comes at the expense of spatial resolution. The detector consists of two sensors tiled next to each other with a 1-pixel dead area. Each sensor has an active area of 12 cm × 14 cm to give a total area of 24 cm x 14 cm with an effective resolution of 2786×2400 pixels and the pixel pitch is 50 µm. The sensor has a quantum efficiency of 50 % at 540 nm, the image depth of analogue-to-digital converter (ADC) is 14-bit and the noise of the sensor with new dedicated readout electronics was improved from the original reported value of 70 electrons rms (root mean square) to be 40 electrons rms, as measured by the photon transfer curve (PTC) method [15].

The characterisation was obtained according to guidelines of the published International Electrotechnical Commission (IEC 62220-1 (2003)) standard that contains a standardised methodology for digital detector characterisation. The measurement uncertainty for DQE, MTF and NNPS was calculated by repeating the measurements three times.

2.1. Beam Quality

The characterisation was performed at University College London (UCL) laboratory with an X-ray source (HS-MP1, Ago X-ray limited, England) of focal spot 1 mm, and a tungsten target with aluminium filtration (W/Al). The measurements were completed using three

Journal Pre-proof

different standard beam qualities: RQA3 (50 kV), RQA5 (70 kV) and RQA7 (90 kV) as RQA3 is suitable for pediatric extremities imaging, while RQA5 is applicable for adult extremity radiography and RQA7 is commonly employed for CBCT imaging. The test geometry was compliant with IEC 62220-1 (2003) standard. The detector was placed at a distance of 150 cm from the X-ray source. This was to ensure beam uniformity on the detector surface. The half value layer (HVL) was measured to determine the beam energy required for measurements for each beam condition using our source [16].

2.2. Signal transfer property (STP)

The STP describes the relationship between the detector mean pixel value (MPV) and air kerma (K_a) to determine how the detector responds to the input signal. Ideally, the response should be linear without any image processing apart from non-uniformity correction and pixel defect calibration [16]. The mean pixel value was studied, in addition to the detector's response fit using Eq 1:

$$MPV = B\,K_a + A \qquad (1)$$

Where A and B are offset and STP gradient of the fit parameters respectively.

2.3. Normalised Noise Power Spectrum (NNPS) Determination

The NNPS determines the relative noise properties in detector response [17]. For this measurement, 30 dark and 30 bright images (across a range of tube currents) were acquired below the saturation level. A second-order polynomial fit was applied to correct the beam non-uniformity. The noise power spectrum (NPS) analysis was conducted according to the IEC protocol by dividing an image into a number of squares referred to as regions of interest (ROIs). Each of these measured 256 × 256 pixels with overlapping of 128 pixels. The NPS was acquired as a function of spatial frequency by applying the fast Fourier transform (FFT) [18,19] using Eq 2:

$$NPS(u,v) = \frac{\Delta x \Delta y}{M N_x N_y} \sum_{m=1}^{M} \left| FFT\{I(x_i,y_i) - S(x_i,y_i)\} \right|^2 \qquad (2)$$

Where u and v are the spatial frequencies reflecting x and y, Δx and Δy are pixel pitches in x and y directions, Nx and Ny express the ROI size in x and y directions, M is the ROIs number which is used in averaging and S(x,y) and I(x,y) are the fitted 2D function and corrected flat field image respectively. The NNPS was obtained by Eq 3:

$$NNPS = \frac{NPS}{(large\ area\ signal)^2} \qquad (3)$$

The large area signal corresponds to the MPV in the image for each dose obtained from STP.

The coefficient of variation (CoV(%)) was calculated by dividing the standard deviation of the pixel values in the image by the mean pixel value. This was included to compare the detector to other commercially available detectors for CBCT applications.

2.4. Pre-sampling Modulation Transfer Function (pMTF) Determination

The pMTF quantifies the resolution of an X-ray detector [20]. To measure the vertical pMTF the polished edge of a tungsten test device, tilted by an angle of 2˚ relative to the pixel rows was placed between two thick lead plates and attached directly to the digital detector. Thirty images were captured at the highest current before saturation for each RQA to decrease the statistical noise. Afterwards, the test device was rotated 90˚ clockwise to measure the horizontal pMTF. Finally, the pMTF was obtained in the frequency domain by fast Fourier transform (FFT) of the line spread function (LSF) which is the derivative of the

Journal Pre-proof

edge spread function (ESF). The pMTF values were calculated from zero to the Nyquist frequency and the pMTF at zero spatial frequency was normalised to one [18,19].

2.5. Detective Quantum Efficiency (DQE) Measurement

DQE is defined as the ability of an imaging system to transfer the input signal to an image [21,22]. It was computed using the following equation (Eq (4)):

$$\mathrm{DQE}(f) = \left(\frac{SNR_{\mathrm{Out}}}{SNR_{In}}\right)^2 = \frac{pMTF^2(f)}{\frac{\Phi}{K_a} * \mathrm{K}_a * NNPS(f)} \qquad (4)$$

Where SNR_{Out}^2 is signal-to-noise ratio square of the output signal on the image and is measured from the acquired images by dividing the pMTF^2 by the averaged NNPS of the digital X-ray imaging device. The SNR_{In}^2 is signal to noise ratio square of the input signal to a detector which can be estimated by multiplying the photon fluence per exposure ratio $\left(\frac{\Phi}{K_a}\right)$ in photons per $\mathrm{mm}^2/\mu\mathrm{Gy}$ by air kerma in µGy where $\left(\frac{\Phi}{K_a}\right)$ values were provided by IEC 62220-1 (2003). It was assumed that the detector behaves as an ideal photon counter [4,23,24].

2.6. Accumulation of Dark Current

This indicates the accumulation of dark charge in the pixel as a function of the integration time. It was measured using the following equation (Eq (5)):

$$i_d = \frac{\overline{S}_{\mathrm{d}} \times K \times q_e}{A \times T_{int}} \qquad (5)$$

Where i_d (A/cm²) is the accumulation of dark current within the pixel, $\overline{S}_{\mathrm{d}}$ (digital number (DN)) is the mean dark signal at different integration times, K (e^-/DN) is the conversion gain, q_e is the electron charge which equals to $1.6\mathrm{x}10^{-19}$ coulombs, A is the pixel area (cm²) and T_{int} is the integration time (s) [24].

The effectiveness of dark frame subtraction, which is the first step in flat field correction, was assessed in terms of fixed pattern noise removal by subtracting two consecutive images having the same exposure time [26].

3. Results and Discussion

3.1. Signal Transfer Property (STP)

Fig. 1 describes the relationship between the K_a and MPV for all RQAs. The detector responded linearly at least within the range of investigated exposures (0.26-2.17µGy for RQA3 and 0.29-1µGy for RQA5,7) with the coefficient of determination (R²) more than 0.9995 in all cases. We observe a signal increase as the beam energy increases. As reported by [23,27], one explanation can be that the photon fluence per exposure ratio increases as the radiation energy increases, therefore, more signal carriers (X-ray photons) are travelling towards the detector as the energy increases. In our case, the signal per unit air kerma increased from 3387.5 X-rays/ mm2/µGy at RQA3 to 9602.8 X-rays/ mm2/µGy at RQA7. Alternatively, it could be that the production of the optical light in the scintillator is taking place closer to the sensor surface as the beam energy increases resulting in more light collection [28]. It is very noticeable that Lassena (CsI) has a high degree of sensitivity to radiation compared to other detectors [11,23,29]. It saturates at 2.17, 1.02 and 0.93 µGy for 54 (RQA3), 74 (RQA5) and 92 kV (RQA7) respectively whereas in general radiography, using digital X-ray detectors, the K_a levels usually range from 0.8 to 8 µGy [30]. However, Lassena (CsI) can provide a satisfactory image quality at low exposures as will be explained in section 3.4. This, therefore, offers the potential to reduce the patient dose.

Journal Pre-proof

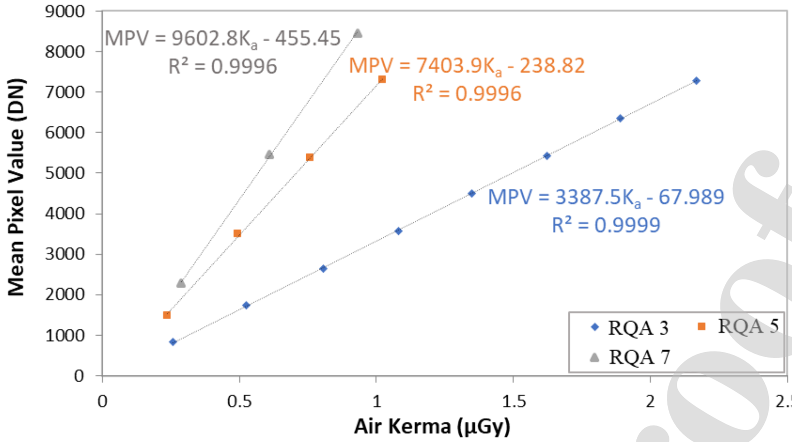

Fig. 1 The relationship between the MPV and K_a for all three energies.

3.2. Pre-sampling Modulation Transfer Function (pMTF)

It was found that the pMTFs are independent of the beam quality within the investigated range (Fig. 2). Increasing the radiation energy slightly improved the resolution at low frequencies between 1 and 3 lp/mm. This is attributed to the longer mean free path of the higher energy X-rays resulting in a greater number of interactions closer to the sensor, which limited the spread of the scintillation photons [23]. The pMTF reaches 50% at 0.9, 1.08 and 1.1 lp/mm for 54, 74 and 92 kV beam qualities respectively (Fig.2). As mentioned before, the frequency corresponding to 10 % MTF describes the limiting resolution of a system and it is around 3 lp/mm for all three beam qualities. In general radiography, the adequate limiting resolution for a detector ranges between 3 and 5 lp/mm [8,23]. Lassena (CsI) was compared to other available CBCTs on the market, the results are illustrated in table 1 [31-35]. The small pixel size gives Lassena (CsI) better resolution. For radiographic imaging comparison, table 2 [11,23,29] shows that Lassena (CsI) has modest pMTF resulting from the scintillator thickness that increases volumetric space for light to spread and scatter [17].

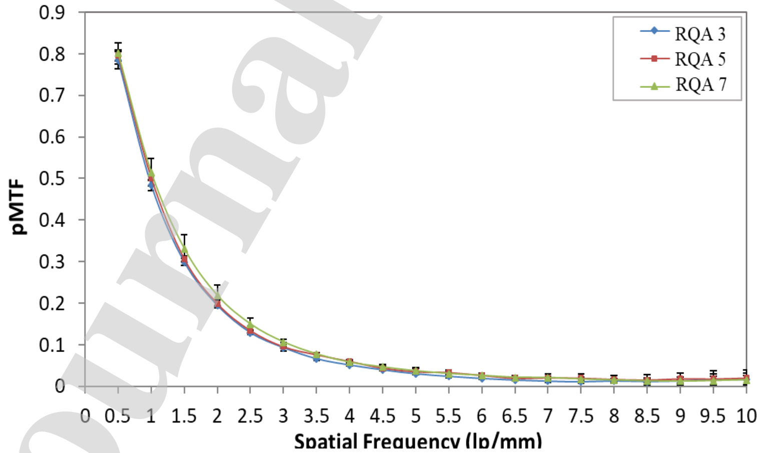

Fig. 2 The averaged pMTFs for Lassena (CsI) at three different energies.

3.3. Normalised Noise Power Spectrum (NNPS)

For the detector under investigation, the NNPS at different energies demonstrated that the NNPS decreased as the radiation energy and dose (or K_a value) increased as shown in Fig. 3. This reduction is due to the intensification of the signal due to the higher number of photons interacting with detector material. Therefore, the number of absorbed photons increases [26,27]. This finding implies that NNPS heavily depends on exposure, consequently, it is expected that the DQE will increase at a higher dose since the DQE is inversely proportional to NNPS.

Lassena (CsI) has a CoV of 0.11% and it is the lower than other commercially available detectors for CBCT applications as displayed in table 1.

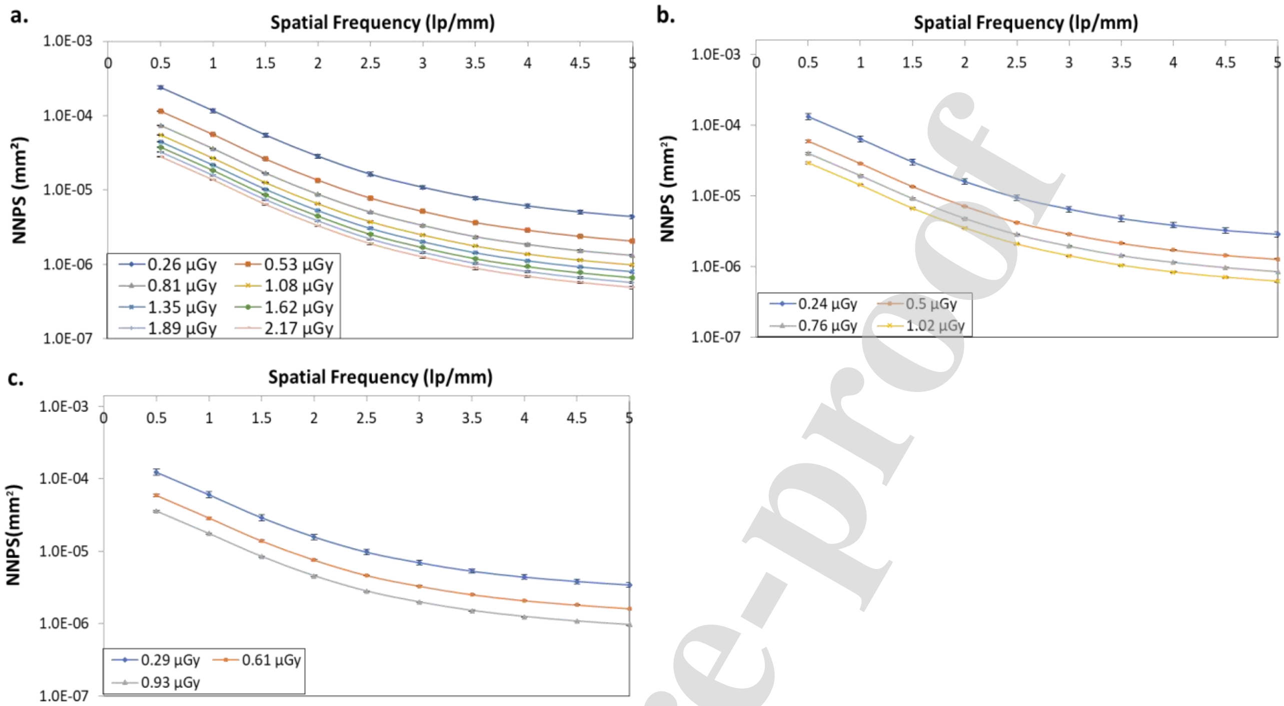

Fig. 3 1D NNPS of a. RQA3 (54 kV) b. RQA5 (74 kV) c. RQA7 (92 kV) at different K_a values.

3.4. Detective Quantum Efficiency (DQE)

We found that the DQE at the three radiation energies reduced as a function of spatial frequency and at high frequencies, the DQE became less exposure dependent due to the increase of the photon shot noise and decrease of the pMTF [26,27]. On the other hand, DQE improved when the radiation current (dose) and voltage (energy) rose as shown in Fig. 4. The DQE (0.5) values are around 0.46 for all doses for RQA3 and they range from 0.52-0.56 for RQA5, lastly, the values of DQE (0.5) for RQA7 are about 0.55-0.59. We can observe that the investigated system demonstrates a quantum-limited condition for RQA3, in other words, it is less exposure dependent at low energies due to remnant fixed pattern noise (FPN) or due to the increased effect of CMOS APS inherent non-linearity as proved by [18]. However, the detector shows higher DQE values at higher energies [36-38]. Looking at table 2, Lassena (CsI) provides acceptable DQE values at low exposures as a detector for general radiography.

Journal Pre-proof

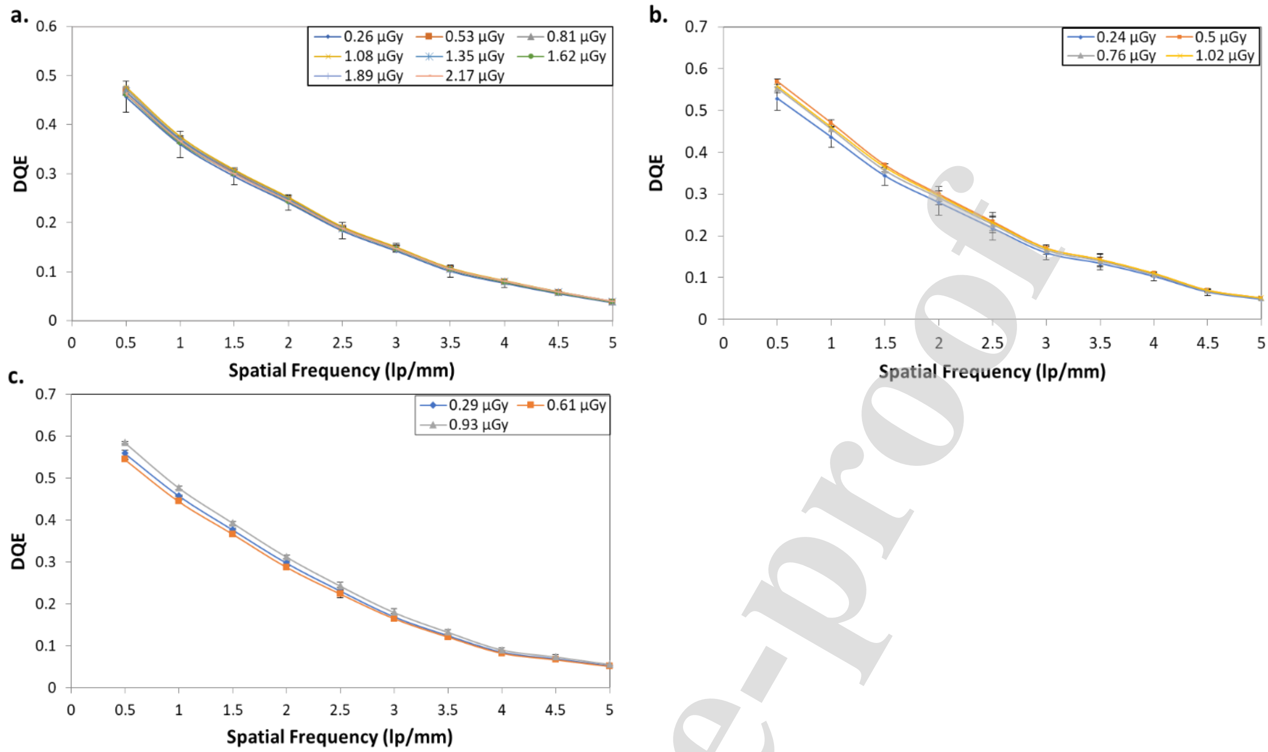

Fig. 4 DQE of a. RQA3 (54 kV) b. RQA5 (74 kV) c. RQA7 (92 kV) at different K_a values.

Table 1 Comparison between the Lassena (CsI) and other available detectors that can be used for CBCT in the radiotherapy departments.

	Varian	Elekta	Siemens	Lassena (CsI)
Resolution (Pixels)	2048 × 1536	1024 × 1024	1024 × 1024	2786 × 2400
Physical size (cm²)	39.73 × 29.8	41 × 41	41 × 41	24 × 14.4
Image depth (bit)	16-bit	16-bit	12/16-bit	14-bit
Pixel pitch (µm)	388	500	400	50
Max frame rate (fps)	30	5.5	25	30
Tube voltage	30-140 kV	70-150 kV	6 MV	54-92 kV
MTF 50%/10% (lp/mm)	0.548/0.939	0.28/0.45	0.3/0.5	1.5/3
Coefficient of variation (%)	0.7%	1.4%	2.7%	0.11%*

*Obtained at the energy of 92 kV and K_a value of 0.93 µGy.

Journal Pre-proof

Table 2 List of Studies that evaluated a new detector and the main findings compared to Lassena (CsI)

		Konstantinidis et al. (2012)	Michail et al. (2015)	Michail et al. (2016)	Lassena (CsI)
Resolution (Pixels)		3888 × 3072	1200 × 1600	1200 × 1600	2786 × 2400
Physical size (cm²)		29 × 23	-	-	24 × 14.4
Image depth (bit)		14-bit	-	-	14-bit
Pixel pitch (µm)		74.8	22.5	22.5	50
Max. frame rate (fps)		26	-	-	30
Scintillator material		CsI:Tl	CsI:Tl	CsI:Tl	CsI:Tl
Scintillator thickness (µm)		200	170	490	1000
MTF 50%/10% (lp/mm)		1.2/4.5	3.6/9.6	1.9/5.8	1.5/3
DQE at 0.5 lp/mm	*RQA3*	0.53-0.68	-	-	0.45-0.47
	Range of dose (µGy)	0.14-3.09	-	-	0.26-2.17
	RQA5	0.68-0.75	0.1	0.8	0.52- 0.56
	Range of dose (µGy)	0.13-6.45	31.05	8.39	0.24-1.02

3.5. Accumulation of Dark Current

The accumulation of dark current was calculated using Eq (5) and it is 2.51 pA/cm^2 for 50 µm pixel pitch system; equivalently, the detector accumulates 391.3 e$^-$/s in the absence of the illuminations. In this case, we measured 12798 e$^-$ at 0.04 s and 14074 e$^-$ at 3.3 s (see Fig. 5). The integration time of the current study was selected at 0.13 s [25,26].

Furthermore, the effectiveness of the fixed-pattern noise correction using dark signal noise (DSN) subtraction was assessed. It was found that the correction removed 99.7 % of the dark fixed-pattern noise as expected [26]. The mean noise dropped from 2053 DN to 4.3 DN after the correction at the selected integration time (0.13 s) (see Fig. 6). This proves the effectiveness of the DNS subtraction for fixed-pattern noise correction.

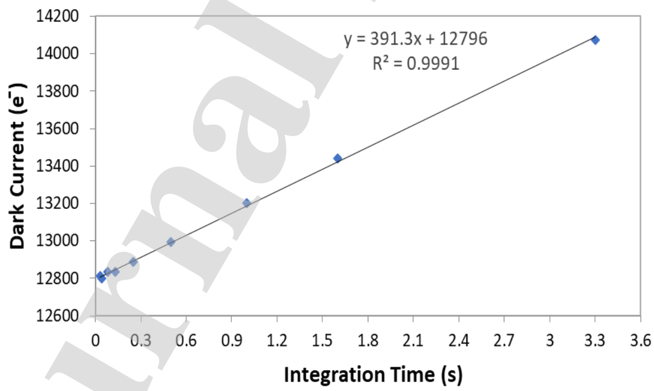

Fig. 5 The relationship between the integration time and the dark current in the absence of illumination.

Journal Pre-proof

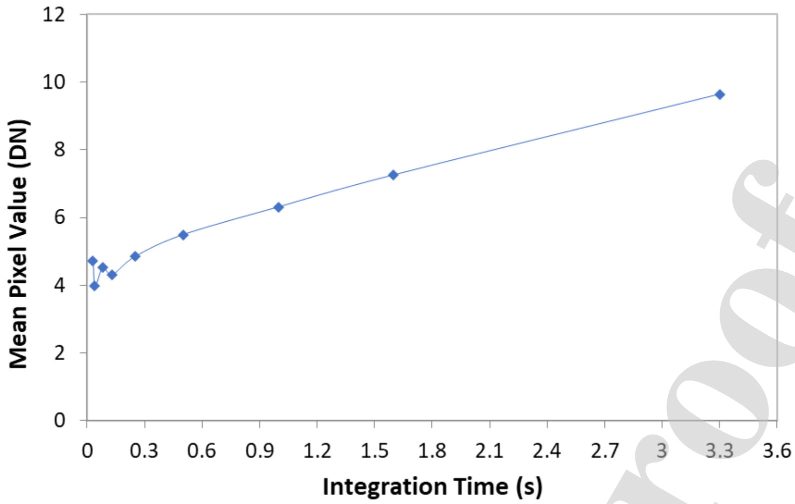

Fig. 6 The difference of two subsequent DNS images as a function of exposure time.

3.6. Role of Scintillator (CsI) in Lassena Performance

The performance of this detector system should be considered in terms of the scintillator (CsI) and the sensor (Lassena) because there are additional factors could degrade the image quality if the sensor is not optimally designed. The Lassena CMOS sensor has 40 e- rms noise while the more ubiquitous a-Si:H detectors have typical noise values of 800-1000 e- rms [39]. The Rose criterion states a resolvable signal needs to be 5 times the noise level to be resolved [40]. For Lassena which has a quantum efficiency of 50%, a point source would need to emit 400 optical photons to be resolved while an a-Si:H detector would need 8000 optical photons. This low noise performance comes at the cost of dynamic range, Lassena has a full well capacity of 112,000 e- and as shown in section 3.1 a bright scintillator such as CsI(Tl) will result in Lassena quickly saturating. The dynamic range of Lassena could be significantly increased by using a dimmer scintillator, but if the absorption remains the same then the noise at lower flux will increase. Ideally, a scintillator with higher absorption with a lower light yield would be preferred. Since low noise digital sensors such as Lassena are relatively new to the market, no such scintillator is available in a suitable form for imaging. There are many alternative scintillators in common use for other applications which have higher X-ray absorption properties and lower light yields, but the K-edge location of the elements that compose the scintillator is crucial for efficiency (Fig. 7). The Fig. 7 shows that energies above 70 keV alternative scintillators begin to show a significant increase in SNR compared to CsI (Tl) in terms of X-ray absorption.

The calculation of how signal and associated noise propagate through each stage of the entire imaging system is known as quantum accounting and allows regions which limit the DQE to be identified [41]. This approach has shown the benefit of increased X-ray absorption in improving DQE. Traditionally the signal transfer stages that limit the DQE also known as the quantum sinks have typically been in the collection of the optical light from the scintillator. In other scintillator based detector systems, the quantum sink associated with the collection of scintillation light, has been a result of the poor efficiency of lens-based systems or high noise of the image sensors. Given the very low noise of Lassena, the X-ray absorption of the scintillator is the most significant factor in limiting the performance of Lassena and a high gain optical stage i.e. bright scintillator is no longer beneficial but instead severely limits the dynamic range of the system.

Journal Pre-proof

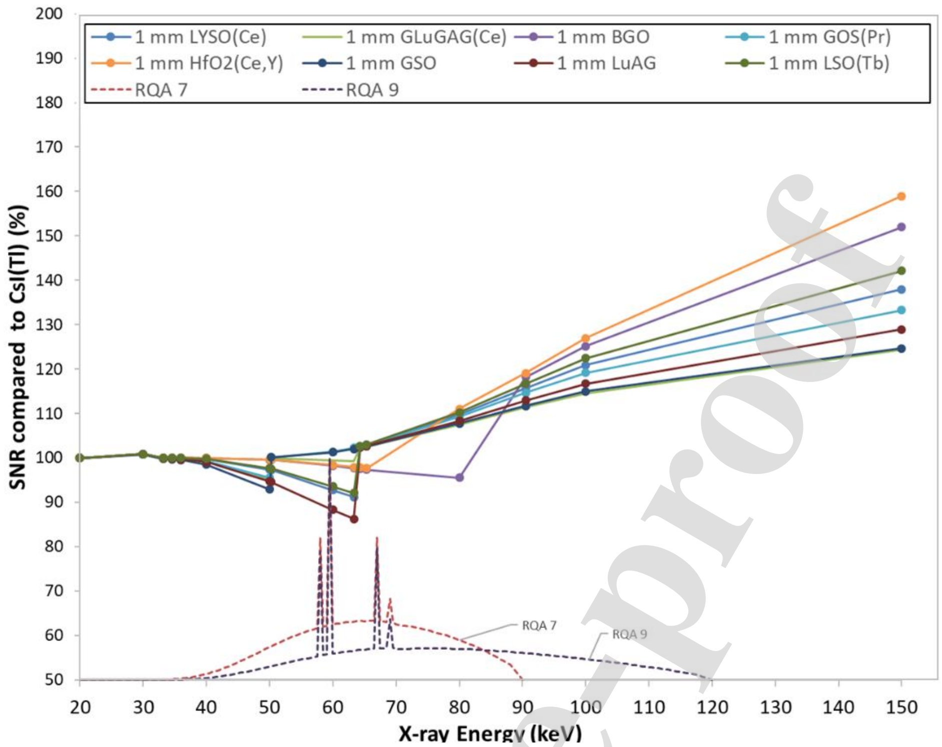

Fig. 7. The percentage difference in signal to noise ratio associated with X-ray absorption in common and uncommon scintillators compared to CsI(Tl). The RQA 7 and 9 spectra are overlaid on the figure for reference.

4. Conclusions

In this paper, a characterisation of the detector Lassena (CsI) performance was realised for the first time over a range of radiation energies and currents to determine its image quality as a detector for general radiography and CBCT applications. The detector responded linearly within the investigated dynamic range however it has very high radiation sensitivity which limited its dynamic range. Despite the scintillator thickness, this system presents a good limiting resolution (3 mm/lp) for a medical imaging application. The thick scintillator improves the SNR but also limits the dynamic range. The spatial resolution and NNPS results led to acceptable DQE at all energies, DQE (0.5) values were 0.46 for RQA3, 0.52-0.56 for RQA5 and 0.55-0.59 for RQA7 at an integration time of 0.13s. For CBCT applications, Lassena (CsI) showed very promising results, and the development of new scintillators to take advantage of low noise sensors, such as Lassena, could drastically improve the performance of imaging systems based on this type of sensor.

Acknowledgements

The first author is sponsored by the Saudi Arabia government. The detector was provided by the Rutherford Appleton Laboratory (RAL) in Oxford, UK.

References

[1] M. Bertolini, A. Nitrosi, S. Rivetti, N. Lanconelli, P. Pattacini, V. Ginocchi, and M. Iori, “A comparison of digital radiography systems in terms of effective detective quantum efficiency,” *Med. Phys.*, vol. 39, no. 5, pp. 2617–2627, 2012.

[2] K. Kim, “Practical expressions describing detective quantum efficiency in flat-panel detectors,” *J. Instrum.*, vol. 6, no. 11, 2011.

Journal Pre-proof

[3] N. T. Ranger, E. Samei, J. T. Dobbins, and C. E. Ravin, “Assessment of Detective Quantum Efficiency: Intercomparison of a Recently Introduced International Standard with Prior Methods [1],” *Radiology*, vol. 243, no. 3, pp. 785–795, Jun. 2007.

[4] G. Zanella, “DQE as detection probability of the radiation detectors,” *Nucl. Instruments Methods Phys. Res. Sect. A Accel. Spectrometers, Detect. Assoc. Equip.*, vol. 586, no. 2, pp. 372–373, Feb. 2008.

[5] H. Illers, D. Vandenbroucke, and E. Buhr, “Measurement of correlated noise in images of computed radiography systems and its influence on the detective quantum efficiency,” *Med. Imaging 2004 Phys. Med. Imaging, Martin J. Yaffe, Michael J. Flynn, Ed. Proc. SPIE Vol. 5368, 639-647*, vol. 5368, pp. 639–647, 2004.

[6] M. B. Williams *et al.*, “Digital Radiography Image Quality: Image Acquisition,” *J. Am. Coll. Radiol.*, vol. 4, no. 6, pp. 371–388, Jun. 2007.

[7] A. Konstantinidis, *Physical Parameters of Image Quality*, vol. 1. Elsevier B.V., 2014.

[8] J. T. Bushberg, J. A. Seibert, E. M. Leidholdt, and J. M. Boone, *The essential physics of medical imaging*.

[9] H.-S. Park, Hee-Joung Kim, Hyo-Min Cho, Jiyoung Jung, and Chang-Lae Lee, “Measurements and evaluation of the image noise power spectrum for computed radiography,” in *2008 IEEE Nuclear Science Symposium Conference Record*, 2008, pp. 4378–4383.

[10] M. hwa Chi, “Technologies for high performance CMOS active pixel imaging system-on-a-chip,” *Int. Conf. Solid-State Integr. Circuit Technol. Proc.*, pp. 180–183, 1998.

[11] C. Michail, I. Valais, I. Seferis, N. Kalyvas, G. Fountos, and I. Kandarakis, “Experimental measurement of a high resolution CMOS detector coupled to CsI scintillators under X-ray radiation,” *Radiat. Meas.*, vol. 74, pp. 39–46, 2015.

[12] V. V. Nagarkar, T. K. Gupta, S. R. Miller, Y. Klugerman, M. R. Squillante, and G. Entine, “Structured CsI(Tl) scintillators for X-ray imaging applications,” *IEEE Trans. Nucl. Sci.*, vol. 45, no. 3, pp. 492–496, 1998.

[13] R. K. Swank, “Absorption and noise in x-ray phosphors,” *J. Appl. Phys.*, vol. 44, no. 9, pp. 4199–4203, 1973.

[14] G. Lubberts, “Random Noise Produced by X-Ray Fluorescent Screens*,” *J. Opt. Soc. Am.*, vol. 58, no. 11, p. 1475, Nov. 1968.

[15] Sedgwick, I., D. Das, N. Guerrini, B. Marsh, and R. Turchetta. "LASSENA: A 6.7 megapixel, 3 sides buttable wafer-scale CMOS sensor using a novel grid-addressing architecture." In *Proceedings of the 2013 Int. Image Sensor Workshop, Jun*, pp. 12-16. 2013.

[16] IEC, “Medical electrical equipment – Characteristics of digital X-ray imaging devices – Part 1: Determination of the detective quantum efficiency,” 2003.

Journal Pre-proof

[17] E. Samei, "Performance of digital radiographic detectors: quantification and assessment methods," *Adv. Digit. Radiogr. RSNA Categ. course diagnostic Radiol. Phys. 2003*, vol. 27710, pp. 37–47, 2003.

[18] A. Konstantinidis, "Evaluation of digital x-ray detectors for medical imaging applications," *PhD thesis, UCL (University College London).*, 2011.

[19] A. C. Konstantinidis, M. B. Szafraniec, R. D. Speller, and A. Olivo, "The Dexela 2923 CMOS X-ray detector: A flat panel detector based on CMOS active pixel sensors for medical imaging applications," *Nucl. Instruments Methods Phys. Res. Sect. A Accel. Spectrometers, Detect. Assoc. Equip.*, vol. 689, pp. 12–21, 2012.

[20] K. Kohm, L. H. Parkway, and S. Louis, "Modulation Transfer Function Measurement Method and Results for the Orbview-3 High Resolution Imaging Satellite," *Imaging*, pp. 1–6, 2003.

[21] D. P. Jones, *Biomedical sensors*. Momentum Press, 2010.

[22] H. P. Chan and K. Doi, "Studies of x-ray energy absorption and quantum noise properties of x-ray screens by use of Monte Carlo simulation," *Med. Phys.*, vol. 11, no. 1, pp. 37–46, Jan. 1984.

[23] A. C. Konstantinidis *et al.*, "X-ray performance evaluation of the dexela cmos aps x-ray detector using monochromatic synchrotron radiation in the mammographic energy range," *IEEE Trans. Nucl. Sci.*, vol. 60, no. 5, pp. 3969–3980, 2013.

[24] C. E. Dick and J. W. Motz, "Image information transfer properties of x-ray fluorescent screens," *Med. Phys.*, vol. 8, no. 3, pp. 337–346, May 1981.

[25] S. E. Bohndiek *et al.*, "Comparison of Methods for Estimating the Conversion Gain of CMOS Active Pixel Sensors," vol. 8, no. 10, pp. 1734–1744, 2008.

[26] M. Endrizzi, P. Oliva, B. Golosio, and P. Delogu, "CMOS APS detector characterization for quantitative X-ray imaging," *Nucl. Instruments Methods Phys. Res. Sect. A Accel. Spectrometers, Detect. Assoc. Equip.*, vol. 703, pp. 26–32, 2013.

[27] N. W. Marshall, "Detective quantum efficiency measured as a function of energy for two full-field digital mammography systems," *Phys. Med. Biol.*, vol. 54, no. 9, pp. 2845–2861, 2009.

[28] M. Salomoni, R. Pots, E. Auffray, and P. Lecoq, "Enhancing Light Extraction of Inorganic Scintillators Using Photonic Crystals," *Crystals*, vol. 8, no. 2, p. 78, Feb. 2018.

[29] C. Michail *et al.*, "Determination of the detective quantum efficiency (DQE) of CMOS/CsI imaging detectors following the novel IEC 62220-1-1:2015 International Standard," *Radiat. Meas.*, vol. 94, pp. 8–17, 2016.

[30] J. Beutel, *Handbook of medical imaging.* SPIE Press, 2000.

[31] L. Lechuga and G. A. Weidlich, “Cone Beam CT vs. Fan Beam CT: A Comparison of Image Quality and Dose Delivered Between Two Differing CT Imaging Modalities,” *Cureus*, vol. 8, no. 9, 2016.

[32] J. Shepherd, “Applications of linac-mounted kilovoltage Cone-beam Computed Tomography in modern radiation therapy: A review,” *Polish J. Radiol.*, vol. 79, pp. 181–193, 2014.

[33] H. S. Abou-Elenein, E. M. Attalla, H. Ammar, I. Eldesoky, M. Farouk, and M. S. Zaghloul, “Megavoltage cone beam computed tomography: Commissioning and evaluation of patient dose.,” *J. Med. Phys.*, vol. 36, no. 4, pp. 205–12, Oct. 2011.

[34] U. V. Elstrøm, L. P. Muren, J. B. B. Petersen, and C. Grau, “Evaluation of image quality for different kV cone-beam CT acquisition and reconstruction methods in the head and neck region,” *Acta Oncol. (Madr).*, vol. 50, no. 6, pp. 908–917, 2011.

[35] M. F. Chan, J. Yang, Y. Song, C. Burman, P. Chan, and S. Li, “Evaluation of imaging performance of major image guidance systems,” *Biomed. Imaging Interv. J.*, vol. 7, no. 2, 2011.

[36] S. Rivetti, N. Lanconelli, M. Bertolini, and D. Acchiappati, “A new clinical unit for digital radiography based on a thick amorphous Selenium plate: Physical and psychophysical characterization,” *Med. Phys.*, vol. 38, no. 8, pp. 4480–4488, Jul. 2011.

[37] K. A. Fetterly and N. J. Hangiandreou, “Effects of x-ray spectra on the DQE of a computed radiography system,” *Med. Phys.*, vol. 28, no. 2, pp. 241–249, Feb. 2001.

[38] Y. El-Mohri, K. W. Jee, L. E. Antonuk, M. Maolinbay, and Q. Zhao, “Determination of the detective quantum efficiency of a prototype, megavoltage indirect detection, active matrix flat-panel imager.,” *Med. Phys.*, vol. 28, pp. 2538–2550, 2001.

[39] X. Liu, H. Ou, J. Chen, S. Deng, N. Xu, and K. Wang, “Highly Photosensitive Dual-Gate a-Si:H TFT and Array for Low-Dose Flat-Panel X-Ray Imaging,” *IEEE Photonics Technol. Lett.*, vol. 28, no. 18, pp. 1952–1955, 2016.

[40] Bao, Qinan, and Arion F. Chatziioannou. 2010. “Estimation of the Minimum Detectable Activity of Preclinical PET Imaging Systems with an Analytical Method.” *Medical Physics* 37 (11).

[41] Cunningham, Ian, “Applied Linear-Systems Theory.” In *Handbook of Medical Imaging, Physics and Psychophysics, vol.1*, pp. 79–159, 2000.

Journal Pre-proof

Journal Pre-proof

Hanan Alzahrani: Conceptualization, Investigation, Validation, Visualization, Writing- Original draft preparation. **Sion Richards:** Resources, Writing- Reviewing and Editing. **Iain Sedgwick:** Resources, Writing- Reviewing and Editing. **Paul Seller:** Resources. **Anastasios Konstantinidis:** Software, Writing- Reviewing and Editing. **Gary Royle:** Supervision, Writing- Reviewing. **Kate Ricketts:** Supervision, Writing- Reviewing and Editing.

Journal Pre-proof

Journal Pre-proof

***Declaration of Interest Statement**

Declaration of interests

☒ The authors declare that they have no known competing financial interests or personal relationships that could have appeared to influence the work reported in this paper.

☐The authors declare the following financial interests/personal relationships which may be considered as potential competing interests:

Journal Pre-proof